Princeton Plasma Physics Laboratory

PPPL- 5048

PPPL- 5048

Tomographic Inversion Techniques Incorporating Physical Constraints for Line Integrated Spectroscopy in Stellarators and Tokamaks

N.A. Pablant, R.E. Bell, M. Bitter, L. Delgado-Aparicio, K.W. Hill, S. Lazerson, and S. Morita

JUNE 2014

PPPL PRINCETON PLASMA PHYSICS LABORATORY

Prepared for the U.S. Department of Energy under Contract DE-AC02-09CH11466.

Princeton Plasma Physics Laboratory
Report Disclaimers

Full Legal Disclaimer

Trademark Disclaimer

PPPL Report Availability

Princeton Plasma Physics Laboratory:

http://www.pppl.gov/techreports.cfm

Office of Scientific and Technical Information (OSTI):

http://www.osti.gov/scitech/

Related Links:

U.S. Department of Energy

Office of Scientific and Technical Information

Tomographic inversion techniques incorporating physical constraints for line integrated spectroscopy in stellarators and tokamaks[a)]

N.A. Pablant,[1] R.E. Bell,[1] M. Bitter,[1] L. Delgado-Aparicio,[1] K.W. Hill,[1] S. Lazerson,[1] and S. Morita[2]
[1)] *Princeton Plasma Physics Laboratory, Princeton, New Jersey 08543, USA*
[2)] *National Institute for Fusion Science, Toki 509-5292, Gifu, Japan*

(Dated: 18 July 2014)

Accurate tomographic inversion is important for diagnostic systems on stellarators and tokamaks which rely on measurements of line integrated emission spectra. A tomographic inversion technique based on spline optimization with enforcement of constraints is described that can produce unique and physically relevant inversions even in situations with noisy or incomplete input data. This inversion technique is routinely used in the analysis of data from the x-ray imaging crystal spectrometer (XICS) installed at LHD. The XICS diagnostic records a 1D image of line integrated emission spectra from impurities in the plasma. Through the use of Doppler spectroscopy and tomographic inversion, XICS can provide profile measurements of the local emissivity, temperature and plasma flow. Tomographic inversion requires the assumption that these measured quantities are flux surface functions, and that a known plasma equilibrium reconstruction is available. In the case of low signal levels or partial spatial coverage of the plasma cross-section, standard inversion techniques utilizing matrix inversion and linear-regularization often cannot produce unique and physically relevant solutions. The addition of physical constraints, such as parameter ranges, derivative directions, and boundary conditions, allow for unique solutions to be reliably found. The constrained inversion technique described here utilizes a modified Levenberg-Marquardt optimization scheme, which introduces a condition avoidance mechanism by selective reduction of search directions. The constrained inversion technique also allows for the addition of more complicated parameter dependencies, for example geometrical dependence of the emissivity due to asymmetries in the plasma density arising from fast rotation. The accuracy of this constrained inversion technique is discussed, with an emphasis on its applicability to systems with limited plasma coverage.

I. INTRODUCTION

Many types of diagnostic systems in use on tokamaks and stellarators (as well as other systems) make use of 1D imaging or arrays of line-integrated measurements. For plasma properties that are expected to be constant on flux surfaces (or where the poloidal dependence on a flux surface is known) it is possible to determine the local profiles through a tomographic inversion[1]. This paper describes an general inversion process that is well suited for complicated flux surface geometry and which can be used even with poor signal levels or severely limited viewing geometry. It is applicable to a large class of diagnostics and geometries.

This inversion process has been developed for the X-Ray Imaging Crystal Spectrometer (XICS) installed on The Large Helical Device (LHD)[2], and results from this diagnostic will be presented. The XICS diagnostic utilizes a spherically bent quartz crystal to provide a 1D image of line integrated spectra from highly charged impurity species in the plasma. The diagnostic concept has been explained in detail by Bitter *et al.*[3] and a conceptual layout can be found in Ref. 3, Fig. 2. The details of the diagnostic hardware design, configuration and calibration on LHD have been reported previously in Ref. 2.

The XICS system on LHD has been designed to view impurity emission from helium-like Ar^{16+}. A spectral fitting process is used to determine line-integrated plasma parameters from the recorded spectra. Standard Doppler spectroscopy techniques are used to determine the ion-temperature (T_i), poloidal flow velocity (V_P) and the Ar^{16+} density. The electron-temperature (T_e) is found from the relative intensities of $n \geq 3$ dielectronic satellite lines to the resonant emission line.

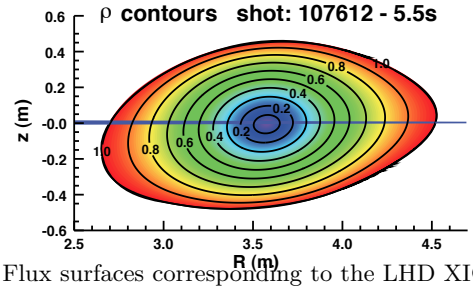

FIG. 1. Flux surfaces corresponding to the LHD XICS sightlines traced through a VMEC equilibrium reconstructed using the STELLOPT[4] software suite. The figure does not represent a planar cut as the XICS sightlines fall on a cone and are not strictly radial. The viewing volume corresponding to a single pixel on the detector is shown in blue and defines the best achievable spatial resolution of the system.

II. INVERSION

Local profiles for the plasma emissivity, temperatures and flow can be found from the line-integrated measurements given the following assumptions: these plasma properties are constant on flux surfaces (or have a known dependence on poloidal angle), and the ion energy distribution is Maxwellian.

The basic process of inversion involves finding a solution for the local profiles that when integrated along the sightlines, reproduce the line-integrated measurements. For Doppler spectroscopy this process can be framed as a matrix inversion problem involving moments of the line integrated spectral lines, as described in Ref. 5,6. For

[a)] Contributed paper published as part of the Proceedings of the 20th Topical Conference on High-Temperature Plasma Diagnostics, Atlanta, Georgia, June, 2014.

the inversion procedure described in this paper, we retain the matrix formulation of the inversion problem and utilize the same set of equations described in the papers referenced above. The present procedure however uses a spline representation for the plasma profiles, and employs a least-squares minimization procedure rather than a matrix inversion approach.

The first step in the inversion process is to define a set of sightlines that correspond to each of the line-integrated measurements, and trace them through a three dimensional reconstruction of the plasma equilibrium[4]. Rather than do a full volume integral, each sightline is approximated as a central line. To obtain a better approximation of the true volume integral that contributes to a given XICS spectrum, multiple sightlines within the volume can be traced and averaged.

To minimize computation time, a pathlength matrix is constructed that can be subsequently used to quickly perform integration in flux space along the sightline. Each element contains the pathlength, in flux space, of a particular sightline through a particular flux zone. Equally spaced flux surfaces, in normalized radius $\rho = \sqrt{\Psi/\Psi_{edge}}$, are used to define the boundaries of each flux zone.

The tomographic inversion is then done in three steps. First the brightness of the resonance and satellite lines are inverted to find the emissivities as a function of flux surface. From the ratio of these inverted emissivities the electron temperature can be determined. Next an inversion of the flow velocity is completed, which requires the inverted emissivity of the resonance line. Finally the ion-temperature can be inverted, which requires both the inverted emissivity and the inverted flow velocity.

For each inversion, the local profile is represented as a quadratic spline with zero derivative at $\rho = 0$. Quadratic splines are chosen in order to simplify the construction of constraints based on the first and second derivatives. A small number of knots, typically between three and five, is used to provide a smooth solution. With sufficient signal quality, additional spline knots can be added to improve the inversion resolution.

The locations of the knots are determined by using a least-squares minimization technique. The residual used for minimization is determined by integrating the local profile along each sightline and comparing against the measured line-integrated profile.

During the minimization process, constraints are imposed in order to ensure that the spline representing the local profile remains realistic and physically plausible. Constraints are imposed through the spline definition, limits on the knot locations and by the implementation of avoidance conditions in the minimization procedure. The implementation of avoidance conditions is described in Section IV.

The resonance and satellite lines are inverted simultaneously to allow for the following shared constraints: 1. The profiles must always be positive. 2. Only a single peak (not necessarily on axis) is allowed in the emissivity profile. This is implemented through derivative constraints. 3. The emissivity of the resonance and satellite lines goes to zero at the same flux surface. While it is possible that the emissivity of the resonance line may go out further than the satellite lines due to recombination of hydrogen-like argon, we expect that this constraint will be a reasonable approximation in most cases. 4. Knot spacing is constrained towards equal spacing in ρ. This constraint, along with the number of chosen knots, acts as a smoothing constraint on the emissivity profile. This is implemented as part of the residual, and a weighting factor controls the amount of smoothing imposed on the profile.

The XICS system on LHD provides a nearly radial view with is insensitive to toroidal flow. In addition the poloidal flow velocity on LHD is significantly larger than the toroidal flow velocity. For these two reasons, we assume a purely poloidal flow in the current work. It is possible however to separate the toroidal and poloidal rotation with an accurate wavelength calibration and a view of both the upper and lower half of the plasma. The unique constraints used during the velocity inversion are: 1. The poloidal flow velocity is zero at the magnetic axis ($\rho = 0.0$). 2. The spline knots are limited to stay within a range of $1/(N_k)$ of their original ρ location, where N_k is the number of knots.

Finally, the following unique constraints are used when inverting the ion-temperature: 1. The profile must always be positive. 2. The first and second derivatives are negative at all values of ρ. 3. The spline knots are limited to stay within a range of $1/(N_k)$ of their original ρ location.

III. CONSISTENCY AND ERROR ANALYSIS

Consistency of the profile models with the measured data can be immediately verified by looking at the final residuals. Any systematic mismatch, outside of the error bars, indicates a problem with the profile models or the equilibrium being used.

Random errors, due to uncertainty in the line integrated measurements, can be addressed using a Monte-Carlo technique. This is done by randomly modifying the points in the line-integrated measurements within their errors, and recomputing the inversion. The result of this type of error analysis is shown in Fig.2 and Fig.3.

Systematic errors due to the profile model, constraints and initial conditions are more difficult to quantify but can be addressed by repeating inversions with different settings and examining the final inverted profiles and the agreement with the measured line-integrated profiles.

IV. MODIFIED LEVENBERG-MARQUARDT MINIMIZATION

The inversion process described in Section II utilizes a modified Levenberg-Marquardt (L-M) algorithm which includes handling of avoidance conditions. The modification provides a general mechanism for preventing the fitting algorithm from entering into parameter spaces where any undesired conditions may occur. Avoidance criteria are implemented by allowing the residual function to return not only an array of residual values, but also an array containing the status of any defined avoidance conditions.

As in a standard L-M fitting routine, a Jacobian is calculated consisting of a matrix of the partial derivatives of each element in the residual with respect to each free parameter. This Jacobian is used to calculate the next L-M step. The residual function is now evaluated using

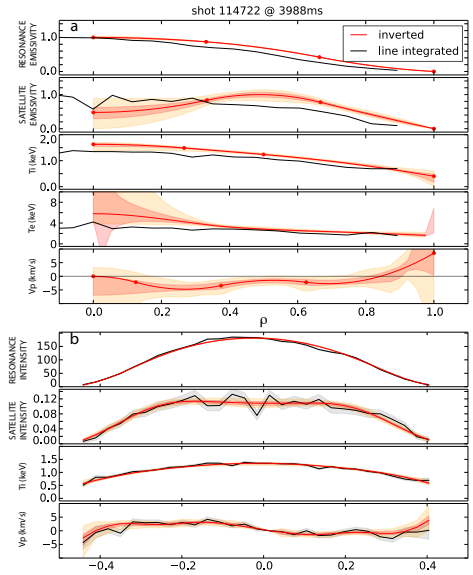

FIG. 2. LHD shot 114722 at 4000ms. Fig a. compares the final inverted plasma profiles (red lines) with the measured line integrated profiles (black lines). Error bars are derived from a Monte-Carlo error analysis. The red shaded region shows the variance in the M-C solutions and is centered about the mean. The yellow shaded region represents the extreme M-C solutions. For the line integrated measurements, the ρ coordinate is taken from the minimum value of ρ that the sightline passes through. The large error bars on T_e near the core are due both to the large error in emissivity of the n=3 satellite lines and to the insensitivity of the T_e calculation above 4keV. Fig. b. compares integrated profiles from the inverted solution and the original measurements. The gray shaded area shows the variance in the line-integrated measurements reported by the spectral fitting algorithm.

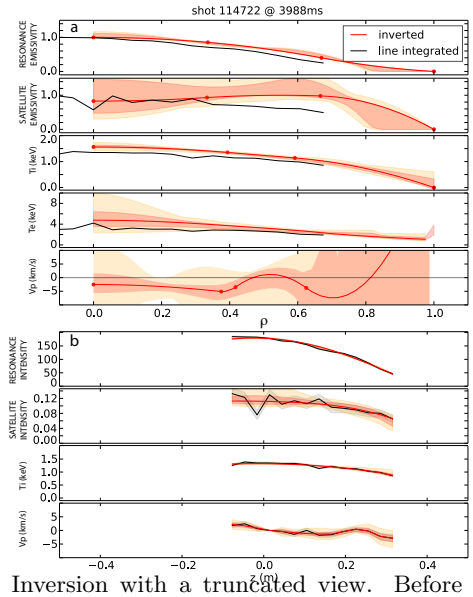

FIG. 3. Inversion with a truncated view. Before performing the tomographic inversion the measured line-integrated profiles from Fig.2 were artificially truncated to simulate a severely limited viewing range. The larger error bars are due both to the limited view and the reduction in the total signal being used.

this step, and returns a residual array and an avoidance array.

It is at this point the standard algorithm is modified. The returned avoidance array is checked for any avoidance conditions. If such conditions exist, then a search is done to find which minimal set of parameters must be frozen to remove the avoidance conditions. These parameters are zeroed out in the Jacobian, effectively treating them as fixed for the remainder of the iteration, and a new L-M step is calculated. During avoidance steps, so long as the residual is reduced, the normal adjustment of the step size based on the predicted and actual residual reduction is disabled.

Once a step has been found that does not lead to an avoidance condition, the L-M algorithm is allowed continue normally by evaluating the summed residuals, checking for convergence and continuing to the next iteration. This process will eventually terminate when any of the convergence criteria are met or no search directions can be found that do not lead to an avoidance condition. If the fitting algorithm terminates with a truncated Jacobian, then iteration is restarted with an additional step: before truncating the Jacobian, the step size is reduced.

At the completion of this minimization process there are four possible outcomes: normal convergence, convergence during a reduced step, convergence with a truncated Jacobian and termination with no valid search directions. All of these outcomes may indicate a successful minimization to a local or global minimum. However, except for normal convergence, it is possible that a better solution exists that could not be reached due to a barrier in parameter space caused by the avoidance conditions.

The modified L-M algorithm is based on `MPFIT`[7] and is available for download at the location in Ref. 8.

ACKNOWLEDGMENTS

The authors would like to thank M. Reinke for many discussions on inversion methods and M. Goto, T. Oishi and the LHD experiment group for their support in the installation of the XICS diagnostic and LHD operation. Research supported by the U.S. DOE under Contract No. DE-AC02-09CH11466 with Princeton University.

[1] M. L. Reinke, Y. A. Podpaly, M. Bitter, I. H. Hutchinson, J. E. Rice, L. Delgado-Aparicio, C. Gao, M. Greenwald, K. Hill, N. T. Howard, A. Hubbard, J. W. Hughes, N. Pablant, A. E. White, and S. M. Wolfe, Review of Scientific Instruments **83**, 113504 (2012).

[2] N. A. Pablant, M. Bitter, L. Delgado-Aparicio, M. Goto, K. Hill, S. Lazerson, S. Morita, A. Roquemore, D. Gates, D. Monticello, G. H. Nielson, A. Reiman, M. Reinke, J. Rice, and H. Yamada, Review of Scientific Instruments **83**, 083506 (2012).

[3] M. Bitter, K. Hill, D. Gates, D. Monticello, H. Neilson, A. Reiman, A. L. Roquemore, S. Morita, M. Goto, H. Yamada, and J. E. Rice, Review of Scientific Instruments **81**, 10E328 (2010).

[4] S. Lazerson and I. Chapman, Plasma Physics and Controlled Fusion **55**, 084004 (2013).

[5] R. E. Bell, Review of Scientific Instruments **68**, 1273 (1997).

[6] I. Condrea, E. Haddad, B. C. Gregory, and G. Abel, Physics of Plasmas **7**, 3641 (2000).

[7] C. B. Markwardt, in *Astronomical Data Analysis Software and Systems XVIII*, Vol. 411 (2009) p. 251.

[8] N. A. Pablant, http://amicitas.bitbucket.org/mirmpfit/ (2014).

Princeton Plasma Physics Laboratory
Office of Reports and Publications

Managed by
Princeton University

under contract with the
U.S. Department of Energy
(DE-AC02-09CH11466)

P.O. Box 451, Princeton, NJ 08543
Phone: 609-243-2245
Fax: 609-243-2751

E-mail: publications@pppl.gov
Website: http://www.pppl.gov